Evaluation of adsorption of surfactant at a moving interface of a single spherical drop

Hosokawa, Shigeo
Hayashi, Kosuke
Tomiyama, Akio

Evaluation of Adsorption of Surfactant at a Moving Interface of a Single Spherical Drop

Shigeo Hosokawa*,**, Kosuke Hayashi*,** and Akio Tomiyama*,**

* Department of Mechanical Engineering, Graduate School of Engineering, Kobe University,
** Complex Fluid and Thermal Engineering Research Center, Kobe University
1-1 Rokkodai, Nada, Kobe, 657-8501, Japan
E-mail: hosokawa@mech.kobe-u.ac.jp

ABSTRACT

Numerical simulations of contaminated bubbles or drops adopt a model of adsorption-desorption kinetics developed for quiescent systems. However, the model has rarely been validated due to the lack of experimental data of surfactant concentration at a moving interface. Hence, we experimentally investigated surfactant concentration at the moving interface of a spherical drop falling in a stagnant liquid containing surfactant using the velocity distributions measured by spatiotemporal filter velocimetry (SFV). The molar flux of surfactant to the interface was also evaluated by substituting the measured velocity and surfactant concentration into the conservation equation of surface concentration of surfactant to examine the applicability of the Frumkin – Levich model to a drop falling in a contaminated system. We confirmed that the evaluation of surfactant concentration using SFV is of great use in understanding adsorption-desorption kinetics at an interface in a contaminated system and for validation of adsorption and desorption models. The measured results showed that the Frumkin – Levich model is not applicable to a moving interface, whereas it is applicable to an immobile interface, that the dependence of the molar flux on the molecular weight of surfactant is not so strong, and that the ratio of the surface concentration of surfactant to the maximum concentration, i.e. the surface coverage, is an appropriate index for judging an applicable range of the Frumkin – Levich model.

Keywords: Drop, Surfactant, Adsorption-desorption kinetics, Interface, Spatiotemporal filter velocimetry

INTRODUCTION

Adsorption of surfactants at an interface changes the interfacial tension and induces the Marangoni stress which affects the boundary condition at the interface and alters interfacial mass and momentum transfer rates. Thus, knowledge on adsorption-desorption kinetics at an interface is of fundamental importance to understand motion and mass transfer of drops and bubbles. Many studies (Levich, 1962; Borwankar and Wasan, 1983; Bleys and Joos, 1985) have been carried out for understanding and modeling adsorption-desorption kinetics. Most of them have dealt with a static interface in a quiescent system. Several numerical simulations (Cuenot et al., 1997; Takagi et al., 2003; Muradoglu and Tryggvason, 2008; Hayashi and Tomiyama, 2012, Dieter-Kissing et al., 2015) have been conducted by using an adsorption-desorption model to predict distributions of surface concentration Γ of surfactant and the Marangoni stress at the moving interface of a bubble or a drop. However, the applicability of the model to the moving interface has rarely been examined due to the difficulty in measuring Γ and the Marangoni stress at the moving interface.

Although there are several methods (Dixon et al., 1949, Takiue et al., 2003, Shen, 1989) for measuring Γ at an interface, few methods (Manning-Benson et al., 1997, Hutchison and Klenerman, 1999, Strickland, et al., 2015) are available for a moving interface. Evaluation of adsorption-desorption model requires measurements of molar fluxes of adsorption and desorption to a moving interface. Evaluation of the molar flux based on the conservation equation of Γ by measuring Γ and interfacial velocity is one of the possible methods. Although Vogel et al. (2001) measured interfacial velocity and Γ using second-harmonic generation (SHG) and boundary fitted DPIV, they did not carry out evaluation of the molar flux of surfactant and validation of available adsorption-desorption models. Hosokawa et al. (2017) proposed an evaluation method of Γ based on accurate velocity measurement using spatiotemporal filter velocimetry (SFV), and demonstrated its validity. Since the method provides interfacial velocity and Γ distributions, it can be used for evaluation of the molar flux.

In this study, we applied the method to the moving interface of a spherical drop falling in a stagnant liquid containing surfactant to measure the molar flux of surfactant to the interface, which was evaluated

by substituting the measured velocity and surfactant concentration into the conservation equation of Γ. The applicability of the Frumkin – Levich model to a drop falling in a contaminated system was discussed based on the experimental results.

EXPERIMENTAL APPARATUS

Figure 1 shows a schematic of the experimental setup. Silicone oil (Shinetsu, KF-96-300cs, density ρ_C: 967 kg/m^3, viscosity μ_C: 299 mPa·s) was filled in the rectangular container of 170 (D) x 170 (W) x 500 mm (H). A drop of glycerol-water solution (53.5 wt%, diameter d: 8.3 mm, density ρ_D: 1132 kg/m^3, viscosity μ_D: 6.13 mPa·s) was released from the nozzle (inner diameter: 5.0 mm) located 450 mm above the bottom of the container at the center of the cross-section. Water purified by using a Millipore system (Elix 3) and pure glycerol (Kishida-Kagaku) were used for the glycerol-water solutions. The concentration of the glycerol-water solution was determined so as to make its refractive index the same as that of the silicone oil to eliminate optical distortion of tracer-particle images in the drop (Ninomiya and Yasuda, 2006). The drop diameter and fluid properties were selected so as to keep the drop Reynolds number Re ($=\rho_C V_T D/\mu_C$) less than unity, to make the wall (container size) effect negligible, and to keep enough measurement resolution to the drop size. Triton X-100 was selected and solved into the glycerol-water solution as surfactant since it has been frequently used in researches on effects of surfactants on the dynamics of bubbles and drops (e.g. Bel Fdhila & Duineveld, 1996; Duineveld, 1998; Zhang et al., 2001; Takagi et al., 2003; Tagawa et al., 2014). SiC particles (mean diameter: 3.0 μm, density: 3210 kg/m^3) were added to both phases as tracer particles after cleaning by mixing with water and ethanol to elute water-based and oil-based contaminants, respectively. Note that the migration of the tracer particles due to the gravity is negligibly small compared with the drop velocity. Fluorescent dye (Rhodamine B, concentration: 5.0 x 10^{-3} mol/m^3) was solved in the glycerol-water solution to identify the drop region in recorded images. The concentration was the minimum concentration at which the drop region could be identified in the images recorded by the present imaging system. The drop shape was spherical and the temperature was 25 $\pm$ 0.5 ^{o}C. Note that the

velocity distribution about a clean spherical drop in the present experimental apparatus was confirmed to agree well with the Hadamard – Rybczynski solution (Hosokawa et al., 2017).

Since the drop reached the terminal velocity at 30 mm below the nozzle tip in the clean system, measurements were carried out at 30 and 40 mm below the nozzle tip. The measurement region at each elevation was ±10 mm in the vertical direction. A laser sheet (wavelength: 532 nm, power: 2W, thickness: 0.2 mm) was introduced from the bottom of the container and particle images were recorded by the high-speed camera (Photron FASTCAM SA-X2, frame rate: 12,500 fps, resolution: 20 μm/pixel) at each elevation. Another camera was located at the position perpendicular to the high-speed cameras to confirm that the laser sheet passed through the center of a drop. For time-series particle images measured at each elevation, we carried out image processing in the following steps; (1) discrimination of the drop region utilizing the fluorescent intensity from Rhodamine B in the drop, (2) calculation of the drop center and interface detection, (3) generation of boundary-fitted measurement regions in the Lagrangian coordinate fixed at the drop center, and (4) velocity evaluation at each measurement region. Spatiotemporal filter velocimetry (SFV) with boundary fitted measurement regions (Hosokawa et al., 2017) was adopted for the accurate velocity measurement in the vicinity of a drop interface. The uncertainty at 95% confidence in the measured instantaneous velocity was less than 5% (Hosokawa and Tomiyama (2012)). Velocities averaged in the measurement regions (±10 mm) were calculated using over 100 instantaneous data for each interrogation area, and the uncertainty in the averaged velocity was less than 0.5%. Details of SFV can be found in Hosokawa and Tomiyama (2012) and Hosokawa et al. (2017).

Figure 2 shows examples of the pathlines and the velocity distribution averaged in the measurement region. V_D in the figure indicates the drop velocity. Surface concentration Γ of the surfactant was calculated from the measured velocity distribution in the vicinity of the interface. First, the interfacial viscous stresses $\tau_{r\theta}$ in both phases were evaluated from the radial gradient of the tangential velocity v_θ measured in the vicinity of the interface and the tangential component of interfacial velocity $v_{\theta int}$:

$$\tau_{r\theta} = \mu \left(\left. \frac{\partial v_\theta}{\partial r} \right|_{r=R} - \frac{v_{\theta int}}{R} \right) \tag{1}$$

where r is the radial coordinate and R the drop radius. Note that $v_{\theta int}$ was evaluated as the average of values extrapolated from inside and outside radial distributions of tangential velocity in the vicinity of the interface by using least square fitting. The difference $\Delta\tau_{r\theta}$ in $\tau_{r\theta}$ between the inside and outside of the drop interface, $\tau_{r\theta,in}$ and $\tau_{r\theta,out}$, indicates the sum of the other forces acting on the interface such as the Marangoni stress and the stress due to surface viscosity. In the present system, we confirmed that the Marangoni stress is main component of $\Delta\tau_{r\theta}$ and the other stresses are negligible (Hosokawa et al., 2017). Hence, $\Delta\tau_{r\theta}$ was regarded as the Marangoni stress hereafter. Since the Marangoni stress is caused by the gradient of interfacial tension σ, the difference between σ and the interfacial tension σ_T at the drop nose can be evaluated by integrating the following relation between $\Delta\tau_{r\theta}$ and σ gradient:

$$\Delta\tau_{r\theta} = \boldsymbol{e_\theta} \cdot \nabla_S \sigma = \frac{1}{R}\frac{\partial \sigma}{\partial \theta} \tag{2}$$

where $\boldsymbol{e}_\theta$ is the unit vector in the azimuthal direction, θ the angle from the nose of the drop and ∇_S the surface gradient. Figure 3 shows an example of measured $v_{\theta int}$, $\partial v_\theta / \partial r$, $\Delta\tau_{r\theta}$ and σ–σ_T. Note that the black and gray curves in Fig. 3 represent the Hadamard – Rybczynski and Stokes solutions, respectively. The measured results in the front and rear parts of the drop agree well with the Hadamrd – Rybczynski solution and the Stokes solution, respectively. $\sigma - \sigma_T$ is zero and constant in the front region. The surface concentration Γ was evaluated from σ using the Frumkin equation (Rosen and Kunjappu, 2012):

$$\sigma(\Gamma) = \sigma_0 + R_G T \Gamma_{max} ln\left(1 - \frac{\Gamma}{\Gamma_{max}}\right) \tag{3}$$

where σ_0 is the interfacial tension in a clean system, R_G the universal gas constant, T the temperature, and Γ_{max} the maximum surface concentration of surfactant. The constant $\sigma - \sigma_T$ in the front region indicates that Γ is constant in this region. The non-zero $v_{\theta int}$ in the front region of the drop induces Γ gradient if Γ is not zero. Hence, the constant Γ in the front region indicates that Γ is zero, i.e., the interface is clean in the front part of the drop. The same results were observed in the present experimental conditions. Thus, σ_T is equal to the interfacial tension σ_0 (3.43×10^{-2} N/m) of a clean interface in the present experiments. An

example of the evaluated Γ is plotted in Fig. 3. The interface is clean (Γ = 0) in the front part and contaminated (high Γ) in the rear part. Note that the results of the numerical simulations by Cuenot et al. (1997) and Bel Fdhila and Duinebeld (1996) show sharp peaks in the viscous stress distributions whereas the present result indicates the relatively smooth distribution. This might be due to the difference in *Re*. In their conditions ($Re = O(10^2)$), strong advection rapidly increases Γ in the transition zone between the clean interface and the stagnant cap regions, and forms a high gradient in Γ which induces a strong peak in the Marangoni stress. The high-speed flow around the bubble quickly decelerated at the interface by the Marangoni stress and the high viscous stress is induced by the deceleration. Even in the present condition, a weak peak in the outside velocity gradient, i.e. viscous stress, can be observed around θ = 140 deg. in Fig .3. Typical uncertainties in $\Delta\tau_{r\theta}$, σ and Γ, which were evaluated by the propagation of uncertainty in the measured velocity, were $2.8\text{x}10^{-1}$ Pa, $6.4 \text{ x } 10^{-4}$ N/m and $2.4 \text{ x } 10^{-8}$ mol/m^2, respectively, and indicated by the error bars in Fig. 3. The variations of the measured data are smaller than the error bars. This indicates that the actual uncertainties in the measured velocity and the other quantities are lower than 5% and the corresponding values, respectively.

Γ_{max} in Eq. (3) was evaluated from the relation between σ and the surfactant concentration *C* in the equilibrium state. σ was measured by using a pendant-drop method (Stauffer, 1965) in a quiescent system of the two fluids. The measured σ decreases with increasing *C* as shown in Fig. 4 and is well fitted by the following Szyszkowski's equation (Rosen and Kunjappu, 2012):

$$\sigma(\Gamma_{eq}) = \sigma_0 - R_G T \Gamma_{max} \ln\left(1+\frac{C}{a}\right) \tag{4}$$

where Γ_{eq} is the equilibrium surface concentration and *a* the ratio of rate constants for adsorption and desorption. Γ_{max} and *a* were evaluated by least square fitting of Eq. (4) to the measured σ, and they were $1.69\text{x}10^{-6}$ mol/m^2 and $1.02\text{x}10^{-3}$ mol/m^3, respectively. σ does not depend on *C* when $C > 2.8\text{x}10^{-1}$ mol/m^3 due to the formation of micelles. Since Eq. (4) is derived from Eq. (3) and the Langmuir isotherm, the good agreement between the measured σ and Eq. (4) implies that Eq. (3) can be used to calculate Γ from σ evaluated using the assumption that the relationship between Γ and σ is the same as that in the equilibrium

state although there is some discussion on applicability of Eq. (3) to various surfactants (e.g. Fainerman et al., 2009) and several accurate models have been proposed (e.g. Kumar, et al., 2003; Krzan et al., 2004).

The experiments were conducted at three different concentrations of the surfactant under the critical micelle concentration as shown in Table 1. Since we assumed that the surface concentration of surfactants is zero at the drop nose, we selected the concentration so as to keep the drop nose clean, which was confirmed in Hosokawa et al. (2017). Γ_{eq} in Case 1, 2 and 3 were 1.12, 1.40 and 1.53x10^{-6} mol/m^2 (66, 83 and 91% of Γ_{max}), respectively. The change in the terminal velocity between two elevations (Y = 30 and 40 mm) was less than 3 % in all conditions. The drop Reynolds number was less than unity in all cases.

RESULTS AND DISCUSSION

Figure 5 shows the measured velocity distributions and pathlines about a drop at Y = 30 and 40 mm for each surfactant concentration C. The drop falls downward and the internal circulation is formed due to the shear stress at the interface. As the drop falls, the surfactant accumulates at the interface of the drop tail, and therefore, the internal circulation disappears in the tail region due to the immobile interface. Thus, the low velocity region is formed in the drop tail. The internal circulation is weaker and the low velocity region is wider at Y = 40 mm than at Y = 30 mm due to accumulation of surfactant at the interface during the translation from Y = 30 to 40 mm. The internal circulation becomes weak and the low velocity region becomes wider with increasing C. These results clearly indicate that the surface concentration Γ changes due to the adsorption and desorption between Y = 30 and 40 mm and the resultant change in the velocity field is successfully captured by SFV.

The measured velocity distributions were compared with the model proposed by Sadhal and Johnson (1983) for a spherical fluid particle with a stagnant cap in the limits of low Reynolds number and high Péclet number. The model gives the following stream functions ψ and $\hat{\psi}$ in outside and inside of the particle:

$$\psi = \left(r^2 - \frac{1}{r}\right)\int_{\cos(\pi-\theta)}^{1} P_1(x)dx + \sum_{k=1}^{\infty} C_k(r^{-k+2} - r^{-k})\int_{\cos(\pi-\theta)}^{1} P_k(x)dx \qquad (r \geq R) \qquad (5)$$

$$\hat{\psi} = \frac{3}{2}(r^4 - r^2)\int_{\cos(\pi-\theta)}^{1} P_1(x)dx + \sum_{k=1}^{\infty} C_k(r^{k+3} - r^{-k+1})\int_{\cos(\pi-\theta)}^{1} P_k(x)dx \qquad (r < R) \qquad (6)$$

where $P_k(x)$ is the kth Legendre polynomial and C_k are given by

$$C_1 = -\left\{\frac{\mu_C}{4\pi(\mu_C + \mu_D)}\left(2\phi + \sin\phi - \sin 2\phi - \frac{1}{3}\sin 3\phi\right) + \frac{2\mu_C + 3\mu_D}{2(\mu_C + \mu_D)}\right\} \qquad (7)$$

$$C_k = -\frac{\mu_C}{4\pi(\mu_C + \mu_D)}\left\{\sin(k+2)\phi - \sin k\phi + \sin(k+1)\phi - \sin(k-1)\phi - 2\left[\frac{\sin(k+2)\phi}{k+2} + \frac{\sin(k-1)\phi}{k-1}\right]\right\}(k \geq 2) \qquad (8)$$

where ϕ is the angle of the stagnant cap region. Figure 6 shows the comparison of the interfacial velocity $v_{\theta int}$ normalized by the drop velocity V_D between the model and the experimental results at $Y = 40$ mm. The measured $v_{\theta int}/V_D$ in the front region agrees with the model in the clean case ($\phi = 0$ deg.), and that in the rear region vanishes due to the formation of stagnant cap. The low velocity region in the rear, i.e. the stagnant cap region, becomes wider as C increases, and therefore, ϕ increases with C. The distribution of $v_{\theta int}/V_D$ and its change with ϕ are well represented by the Sadhal & Johnson model. Judging from the velocity distribution in the transient region between the clean interface and the stagnant cap region, the measured velocity distributions in Cases 1, 2 and 3 correspond to the model results calculated with $\phi = 40$, 60 and 75 degrees, respectively, whereas the model underestimates the maximum velocity at the clean interface. Figure 7 shows comparisons between the velocity distributions measured at $Y = 40$ mm and those calculated by the model. The model well represents the position and strength of the internal circulation, the size of low velocity region in the rear part and the velocity distribution about the drop in spite of its stepwise boundary condition at the interface. This might be due to high viscous diffusion of the momentum at the low Reynolds number. These results indicate that the Sadhal & Johnson model gives reasonable predictions of velocity distribution of a contaminated spherical drop under low Reynolds number and high Péclet number conditions, provided that a reasonable angle of the stagnant cap is given.

Figure 8 shows $v_{\theta int}$, Γ and each term in the conservation equation of Γ:

$$\frac{\partial \Gamma}{\partial t} + \nabla_S \cdot \boldsymbol{v}_S \Gamma = D_S \nabla_S^2 \Gamma + \dot{S} \tag{9}$$

calculated from the data measured at $Y = 30$ and 40 mm. In Eq. (9), $\boldsymbol{v}_S$ is the surface velocity, D_S the diffusion coefficient at the interface and $\dot{S}$ the molar flux of surfactant due to adsorption and desorption. The magnitude of each term was calculated by substituting the measured v_θ and Γ into each term to evaluate $\dot{S}$ as the residual. D_S was assumed to be the same as the diffusion coefficient D in the bulk. The first term in the LHS was evaluated from the difference in the measured Γ and the transit time of the drop center between $Y = 30$ and 40 mm. The advection and diffusion terms were evaluated from the averaged distributions of $\boldsymbol{v}_S$ and Γ measured at $Y = 30$ and 40 mm. Typical uncertainties in $\partial\Gamma/\partial t$, $\nabla_S \cdot \boldsymbol{v}_S\Gamma$, $D_S\nabla_S^2\Gamma$ and $\dot{S}$ were $1.6\text{x}10^{-7}$, $1.3\text{x}10^{-7}$, $2.0\text{x}10^{-10}$ and $2.9\text{x}10^{-7}$ mol/m^2/s, respectively. Γ increases with θ especially in $120 < \theta < 170$, $90 < \theta < 160$ and $60 < \theta < 150$ deg. for cases 1, 2 and 3, respectively. Γ at the drop tail ($\theta = 180$ deg.) approaches the equilibrium value Γ_{eq} as the drop moves from $Y = 30$ to 40 mm. The stagnant cap region in which v_θ vanishes extends toward the drop front and v_θ upstream of the stagnant cap decreases due to the accumulation of surfactant as the drop falls. $\partial\Gamma/\partial t$ takes positive values over the interface and its peak locates around $\theta = 150$, 130 and 120 deg. for cases 1, 2 and 3, respectively. The diffusion term in Eq. (9) is negligible in comparison with the other terms, i.e. the effect of surface diffusion on Γ distribution is negligible. The advection term takes positive values in $\theta < 140$, 120 and 105 deg. for cases 1, 2 and 3, respectively. It takes negative values in the tail region of the drop. The advection decreases Γ in its positive region and increases Γ in the tail region. $\dot{S}$ takes positive values over the interface, which means that the adsorption is larger than the desorption over the interface in the present cases. $\dot{S}$ takes high values especially in the region of positive advection.

The Frumkin – Levich model for a quiescent system is frequently adopted in numerical simulations and analytical derivations of contaminated interfaces (Cuenot et al., 1997; Takagi et al., 2003; Muradoglu and Tryggvason, 2008; Hayashi and Tomiyama, 2012; Dukhin et al., 2016):

$$\dot{S} = k(C_S(\Gamma_{max} - \Gamma) - a\Gamma) \tag{10}$$

where k is the adsorption rate constant and C_S the molar concentration of surfactant in the vicinity of the interface. Note that k is evaluated from measured dynamic interfacial tension, i.e. time history of σ measured by the pendant drop method by the same procedure as Kumar et al. (2003), which also provided the diffusion coefficient D (= 2.0 x 10^{-10} m^2/s). The procedure implied that the adsorption process in the present experimental range was in mixed control. Figure 9 shows the relation between $\dot{S}$ and Γ together with Eq. (10) which is calculated by assuming $C_S = C$. Note that the adsorption is stronger than the desorption in the present system, i.e., $C_S < C$, and therefore, the assumption of $C_S = C$ tends to overestimate $\dot{S}$. The measured $\dot{S}$ agrees with Eq. (10) in the region of $\Gamma > 0.7$ x 10^{-6} mol/m^2, in which v_θ is less than 5% of V_D. This indicates that the Frumkin – Levich model is valid for a stationary interface, and that the present method based on velocity distribution measured by SFV gives reasonable evaluations of $\dot{S}$. On the other hand, the measured $\dot{S}$ is much larger than Eq. (10) in the region of $\Gamma < 0.7$ x 10^{-6} mol/m^2, where v_θ takes higher values. This difference tends to increase when the correct C_S is used for evaluating Eq. (10) to plot the lines in Fig. 9. Thus, this difference is not caused by the assumption of $C_S = C$ and implies that the Frumkin – Levich model underestimates $\dot{S}$ at a moving interface. Although further experiments using various surfactants in various fluid properties are necessary to obtain general characteristics of adsorption to moving interfaces, we could confirm that there is a case in which the Frumkin – Levich model cannot apply for evaluation of $\dot{S}$ to moving interface.

The possible error sources in the estimated $\dot{S}$ could be (1) the use of the diffusion coefficient D of the bulk liquid for D_S in Eq. (9), (2) difference between the interfacial velocity $\boldsymbol{v}_S$ and the velocity of surfactant molecules at the interface due to interaction of the molecules (error in evaluating the advection term) and (3) presence of surface viscosity which induces an error in the Marangoni stress. Since the diffusion term in Eq. (9) is less than 0.1% of the maximum value in $\partial\Gamma/\partial t$, the influence of the use of the bulk diffusion coefficient is negligible. In general, the interaction between molecules and interfacial viscosity become stronger as the molecular weight increases (Sato et al., 1998). We therefore carried out experiments using Triton X-141 (TX-141) as the surfactants, whose chemical properties are shown in Table 2. The results are shown in Fig. 10 together with the results using Triton X-100 (TX-100). Although the molecular weight of

Triton X-141 is about 20% higher than that of Triton X-100, there is no difference in $\dot{S}$ between the two surfactants. This indicates that the sensitivity of molecular weight, i.e., the interaction between molecules and interfacial viscosity is low. Thus, the difference between the measured $\dot{S}$ and Eq. (10) in $\Gamma < 0.7 \times 10^{-6}$ mol/m^2 is not caused only by the above error sources, and it is highly probable that Γ cannot be evaluated by the combination of Eqs. (9) and (10) for mobile interface. Note that, improvements in numerical simulations for bubbles/drops in contaminated systems is required even when the difference between the measured $\dot{S}$ and Eq. (10) is caused by the molecular interaction or the interface viscosity, since they are not taken into account in most of the numerical methods.

The generalized Frumkin model is frequently used for more complex adsorption-desorption kinetics (Chang et al., 1998; Casandra et al, 2017):

$$\dot{S} = k_a exp\left(-\frac{E_a}{RT}\right) C_S(\Gamma_{max} - \Gamma) - k_d exp\left(-\frac{E_d}{RT}\right)\Gamma \tag{11}$$

where k_a and k_d are the adsorption and desorption constants, respectively. E_a and E_d are the activation energies which are frequently given by the exponential function of Γ:

$$E_a = E_{a0} + \nu_a(\Gamma/\Gamma_{max})^n \tag{12}$$
$$E_d = E_{d0} + \nu_d(\Gamma/\Gamma_{max})^n \tag{13}$$

where E_{a0}, E_{d0} and n are the constants and ν_a and ν_d the constants representing the effect of intermolecular interaction on adsorption-desorption kinetics. Substituting Eqs. (12) and (13) into Eq. (11) yields

$$\dot{S} = k_a^* exp\left(-\frac{\nu_a}{RT}\frac{\Gamma^n}{\Gamma_{max}^n}\right) C_S(\Gamma_{max} - \Gamma) - k_d^* exp\left(-\frac{\nu_d}{RT}\frac{\Gamma^n}{\Gamma_{max}^n}\right)\Gamma \tag{14}$$

where $k_a^* = k_a \exp(-E_{a0}/RT)$ and $k_d^* = k_d \exp(-E_{d0}/RT)$. Equation (14) covers many models on the adsorption-desorption kinetics such as models proposed by Kumar et al. (2003) and Lee et al. (2003) as well as the Frumkin-Levich model. By assuming $k_a^* = k$, $k_d^* = k\,a$ and $n = 0.1$, Eq. (14) can be fitted to the experimental data as shown in Fig. 9, where the values of $(\frac{\nu_a}{RT\Gamma_{max}^n}, \frac{\nu_d}{RT\Gamma_{max}^n})$ are (-18.0, -22.0), (-13.0, -21.4) and (-9.4, -19.5) for Cases 1, 2 and 3, respectively. The curves well represent the trend of measured $\dot{S}$ in

the low Γ regions. Hence, Eq. (14) can be used to represent the present experimental results, although further experiments are necessary to clarify the physical mechanism of the high $\dot{S}$ in the low Γ region.

It is important to judge whether $\dot{S}$ can be evaluated by the Frumkin – Levich model or not. Figure 11 (a) shows a comparison of Γ among the three conditions using Triton X-100. When Γ/Γ_{max} is larger than 0.45 (about a half of Γ_{max}), the measured $\dot{S}$ agrees well with the Frumkin – Levich model and depend on *C*. To the contrary, the measured $\dot{S}$ takes higher values than the model and the dependence on *C* is weak in $\Gamma/\Gamma_{max} < 0.4$. $\dot{S}$ takes a peak around $\Gamma/\Gamma_{max} = 0.1$ and decreases as Γ/Γ_{max} decreases. Figure 11 (b) shows the normalized plot of Γ and $\dot{S}$ based on the Frumkin – Levich model. The $\dot{S}$ in the high Γ region agree well with the model, whereas those in the low Γ region take high values. Although the boundary (the arrow position in the figure) between the two regions depends on *C* in Fig. 11 (b), it does not in Fig. 11 (a). Hence, Γ/Γ_{max} is the better index than Γ/Γ_{eq} to judge whether $\dot{S}$ can be evaluated by the Frumkin – Levich model or not. This implies that the applicability of Frumkin – Levich model depends not on the degree of equilibrium but on the surface coverage ratio of surfactants.

Although further experiments are required, some improvement of adsorption – desorption kinetics is definitely required for accurate simulations of a moving interface in a contaminated system.

CONCLUSIONS

The spatiotemporal filter velocimetry (SFV) was applied to a flow about a single drop of glycerol-water solution falling in a stagnant silicone oil. The drop shape was spherical and the drop Reynolds number was less than unity. Triton X-100 was used as the surfactant. The distributions of surface tension and surfactant concentration along the longitudinal line of the interface were evaluated using the velocity distributions in the vicinity of the interface. The magnitude of each term in the conservation equation of surface concentration of surfactant was also evaluated from the data measured at two elevations. The experiments were carried out for three different concentrations of surfactant. Experiments using Triton X-114 was also carried out to examine effect of molecular weight on the molar flux of surfactant to an interface. As a result, we confirmed that (1) the Frumkin – Levich model gives good estimation for the

molar flux of surfactant in the stagnant cap region of the drops, whereas it is not applicable to the moving interface, (2) the generalized Frumkin model gives better fit to the molar flux of surfactant to a moving interface than the Frumkin – Levich model, (3) the dependence of the molar flux on the molecular weight of surfactant is not so strong, and (4) the ratio Γ/Γ_{max} is the better index than the ratio Γ/Γ_{eq} in order to judge whether $\dot{S}$ can be evaluated by the Frumkin – Levich model or not in the present experimental range. These results clearly show that the evaluation of surfactant concentration using SFV is of great use in understanding adsorption-desorption kinetics at an interface in a contaminated system and in validation of numerical simulations taking into account adsorption and desorption of surfactant. Although further experiments using various surfactants in various fluid properties are necessary to obtain general characteristics of adsorption at moving interfaces, we could confirm that there is a case in which the Frumkin – Levich model cannot be applied to the evaluation of molar flux of surfactant at a moving interface.

ACKNOWLEDGEMENT

The authors gratefully acknowledge Mr. Yuya Masukura and Mr. Ryota Okamoto for their efforts in the experiments. This work has been support by Japan Society for the Promotion of Science (grand-in-aid for scientific research (C) No. 16K06083).

Nomenclature

a:	ratio of rate constants for adsorption and desorption	[mol/m^3]
C:	concentration of surfactant	[mol/m^3]
D:	diffusion coefficient	[m^2/s]
d:	drop diameter	[m]
R:	drop radius	[m]
R_G:	gas constant	[J/K/mol]
r:	coordinate in radial direction	[m]
$\dot{S}$:	molar flux of surfactant to an interface	[mol/m^2/s]
T:	temperature	[K]
t:	time	[s]
V_D:	drop velocity	[m/s]
v:	velocity	[m/s]
x:	coordinate in horizontal direction	[m]
Y:	distance from nozzle tip	[m]
y:	coordinate in vertical direction	[m]
$\Delta\tau_{r\theta}$:	Marangoni stress	[Pa]
Γ:	surface concentration of surfactant	[mol/m^2]
μ:	viscosity	[Pa s]
θ:	coordinate in tangential direction	[deg.]
ρ:	density	[kg/m^3]
σ:	interfacial tension	[N/m]
τ:	interfacial shear stress	[Pa]

Subscript

0:	clean system
C:	continuous phase
D:	drop
eq:	equilibrium
in:	inside of drop
max:	maximum
out:	outside of drop
S:	surface
θ:	θ component
θint:	θ component at interface

REFERENCES

Bel Fdhila, R. and Duineveld, P.C., 1996, The effect of surfactant on the rise of a spherical bubble at high Reynolds and Peclet numbers, *Physics of Fluids*, Vol. 8, pp. 310 – 321.

Borwankar, R.P. and Wasan, D.T., 1983, The kinetics od adsorption of surface active agent at gas-liquid surfaces, *Chemical Engineering Science*, Vol. 38, No. 10, pp. 1637 – 1649.

Bleys, G. and Joos, P., 1985, Adsorption kinetics of bolaform surfactants at the air/water interface, *Journal of Physical Chemistry*, Vol. 89, pp. 1027 – 1032.

Casandra A., Chung, M.-C., Noskov, B.A. and Lin, S.-Y., Adsorption kinetics of sodium dodecyl sulfate on perturb air-water interfaces, *Colloids and Surfaces A: Physicochemical Engineering Aspects*, Vol. 518 (2017), pp. 241 – 248.

Chang, H.-C., Hsu, C.T. and Lin, S.-Y., Adsorption kinetics of $C_{10}E_8$ at air-water interfaces, *Langmuir*, Vol. 14 (1998), pp. 2476 – 2484.

Cuenot, B., Magnaudet, J. and Spennato, B., 1997, The Effect of Slightly Soluble Surfactants on the Flow Around a Spherical Bubble, *Journal of Fluid Mechanics*, Vol. 339, pp. 25 – 53.

Dieter-Kissing, K., Marschall, H. and Bothe D., 2015, Direct numerical simulation of droplet formation processes under the influence of soluble surfactant mixtures, *Computers & Fluids*, Vol. 113, pp. 93 – 105.

Dixon, J.K, Weith, A.J., Argyle, A.A. and Salley, D.J., 1949, Measurement of the Adsorption of Surface-Active Agent at a Solution-Air Interface by a Radiotracer Method, *Nature*, Vol. 163, 845.

Dukhin, S.S., Lotfi, M., Kovalchuk, V.I., Bastani, D. and Miller, R., 2015, Dynamics of rear stagnant cap formation at the surface of rising bubbles in surfactant solutions at large Reynolds and Marangoni numbers and for slow sorption kinetics, *Colloids and Surfaces A: Physicochemical and Engineering Aspects*, Vol. 492, pp. 127 – 137.

Duineveld, P.C., 1998, Bouncing and Coalescence of Bubble Pairs Rising at High Reynolds Number in Pure Water or Aqueous Surfactant Solutions, *Applied Scientific Research*, Vol. 58, pp. 409 – 439.

Fainerman, V.B., Lylyk, S.V., Aksenenko, E.V., Makievski, A.V., Petkov, J.T., Yorke, J. and Miller, R., (2009), Adsorption layer characteristics of Triton surfactants 1. Surface tension and adsorption isotherms,

Colloids and Surfaces A: Physicochemical and Engineering Aspects, Vol. 334, pp. 1 – 7.

Hayashi, K. and Tomiyama, A., 2012, Effects of Surfactant on Terminal Velocity of a Taylor Bubble in a Vertical Pipe, *International Journal of Multiphase Flow*, Vol. 39, pp. 78 – 87.

Hosokawa, S., Masukura, Y., Hayashi, K. and Tomiyama, A., 2017. Experimental Evaluation of Surfactant Concentration at an Interface of Single Spherical Drop, *International Journal of Multiphase Flow*, Vol. 97, pp. 157 – 167.

Hosokawa, S. and Tomiyama, A., 2012. Spatial Filter Velocimetry Based on Time-Series Particle Images. *Experiments in Fluids*, Vol. 52, pp. 1361–1372.

Hutchison, J., Klenerman, D., Manning-Benson, S. and Bain, C., 1999, Measurement of the Adsorption Kinetics of a Cationic Surfactant in a Liquid Jet by Ellipsometry, *Langmuir*, Vol. 15, 7530 – 7533.

Krzan, M., Lunkenheimer, K. and Malysa, K., 2004, On the influence of the surfactant's polar group on the local and terminal velocities of bubbles, *Colloids and Surfaces A: Physicochemical Engineering Aspects*, Vol. 250, pp. 431 – 441.

Kumar, N., Couzis, A. and Maldarelli, C., 2003, Measurement of the kinetic rate constants for the adsorption of superspreading trisiloxanes to an air/aqueous interface and the relevance of these measurements to the mechanism of super spreading, *Journal of Colloid and Interface Science*, Vol. 267, pp. 272 – 285.

Lee, Y.-C., Stebe, K.J., Liu, H.-S. and Lin, S.-Y., 2003, Adsorption and desorption kinetics of CmE8 on impulsively expanded or compressed air-water interfaces, *Colloids and Surfaces A: Physicochemical Engineering Aspects*, Vol. 220, pp. 139 – 150.

Levich, 1962, *Physicochemical Hydrodynamics*, Prentice Hall.

Manning-Benson, S., Bain, C.D. and Darton, R.C., 1997, Measurement of Dynamic Interfacial Properties in an Overflowing Cylinder by Ellipsometry, *Journal of Colloid and Interface Science*, Vol. 189, 109 – 116.

Muradoglu, M. and Tryggvason, G., 2008, A front-tracking method for computation of interfacial flows with soluble surfactants, *Journal of Computational Physics*, Vol 227, pp. 2238 – 2262.

Ninomiya, N. and Yasuda, K., 2006, Visualization and PIV Measurement of the Flow around and inside of a Falling Droplet, *Journal of Visualization*, Vol. 9, pp. 257 – 264.

Rosen, M.J. and Kunjappu, J.T., 2012, *Surfactants and Interfacial Phenomena*, Wiley.

Sadhal, S.S. and Johnson, R.R., 1983, Stokes flow past bubbles and drops partially coated with thin films. Part 1. Stagnant cap of surfactant film – exact solution, *Journal of Fluid Mechanics*, Vol. 126, pp. 237 –

250.

Sato, N., Ito, S. and Yamamoto, M., 1998, Molecular weight dependence of shear viscosity of a polymer monolayer: evidence for the lack of chain entanglement in the two-dimensional plane, *Macromolecules*, Vol. 31, pp. 2673 – 2675.

Shen, Y.R., 1989, Surface Properties probed by Second-Harmonics and Sum-Frequency Generation, *Nature*, Vol. 337, 519 – 525.

Stauffer, C.E., 1965, The Measurement of Surface Tension by the Pendant Drop Technique, *Journal of Physical Chemistry*, Vol. 69 (6), pp. 1933 – 1938.

Strickland, S.L., Shearer, M. and Daniels, K.E., 2015, Spatiotemporal measurement of surfactant distribution on gravity-capillary waves, *Journal of Fluid Mechanics*, Vol. 777, 523 – 543.

Tagawa, Y., Takagi, S. and Matsumoto, Y., 2014, Surfactant effect on path instability of a rising bubble, *Journal of Fluid Mechanics*, vol. 738, pp. 124 – 142.

Takagi S, Uda T, Watanabe Y, Matsumoto Y. 2003. Behavior of a rising bubble in water with surfactant dissolution (1st report, steady behavior), *Trans. JSME* B 69:2192–99 (In Japanese)

Takiue, T., Kawagoe, Y., Muroi, S., Murakami, R., Ikeda, N. and Aratono, M., 2003, Surface Density Measurement of the Bromide Ion by the Total-Reflection X-ray Absorption Fine Structure Technique at the Air/Aqueous Dodecyltrimethylammonium Bromide Solution Interface, *Langmuir*, Vol. 19, 10803 – 10807.

Vogel, M.J., Hisa, A.H., Kelley, J.S. and Korenowski, G.M., 2001, Simultaneous Measurement of Free-Surface Velocity and Surfactant Concentration via a Common Laser Probe, *Review of Scientific Instruments*, Vol. 72, Number 2, 1502 – 1509.

Zhang, Y., McLaughlin, J.B. and Finch J.A., 2001, Bubble velocity profile and model of surfactant mass transfer to bubble surface, *Chemical Engineering Science*, Vol. 56, pp. 6605 – 6616.

FIGURE CAPTIONS

Fig. 1 Experimental setup

Fig. 2 An example of measured velocity distribution about single drop.

Fig. 3 Evaluation process of surfactant concentration.

Fig. 4 Effect of C on σ.

Fig. 5 Measured velocity distribution about a drop.

Fig. 6 Measured and theoretical interfacial velocities.

Fig. 7 Measured and theoretical velocity distributions about a drop.

Fig. 8 v_θ, Γ and budget of Γ (a: Case 1, $C = 0.2 \times 10^{-2}$ mol/m^3, b: Case 2, $C = 0.5 \times 10^{-2}$ mol/m^3, c: Case 3, $C = 1.0 \times 10^{-2}$ mol/m^3)

Fig. 9 Relationship between Γ and $\dot{S}$.

Fig. 10 Comparison of $\dot{S}$ between Triton X-100 and X-141.

Fig. 11 Molar flux of surfactant due to adsorption and desorption

Table 1 Experimental conditions

Table 2 Physical properties of surfactants

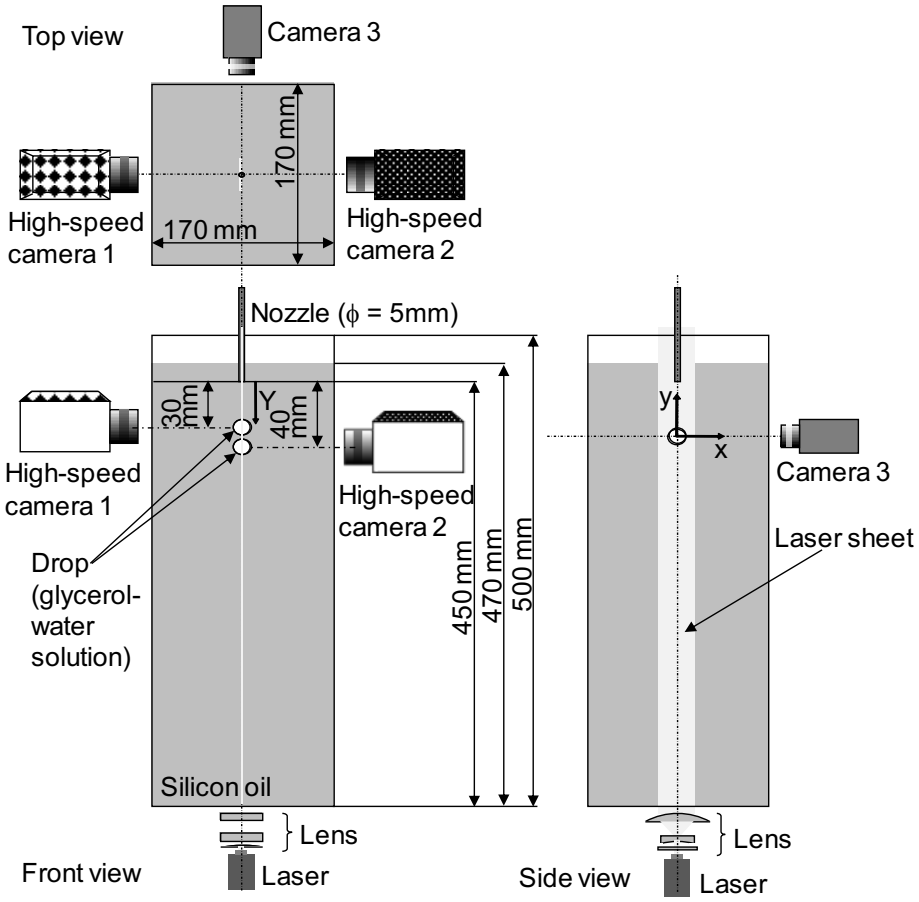

Fig. 1 Experimental setup

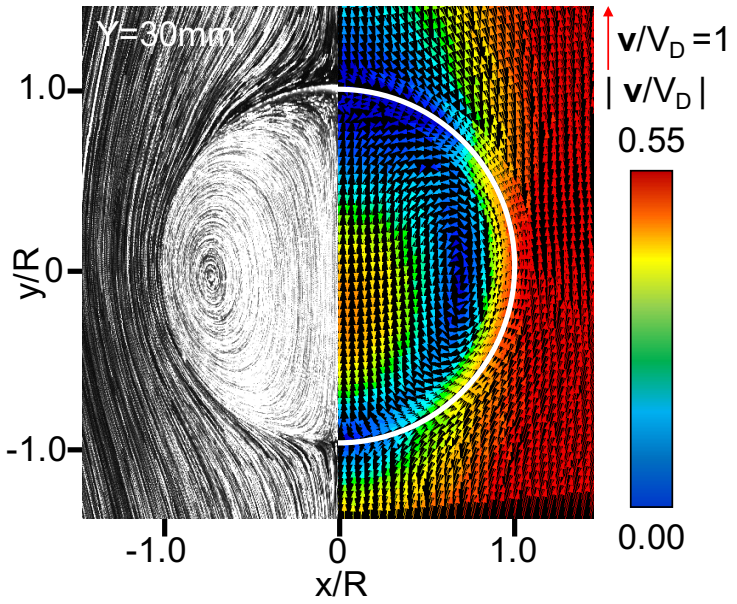

Fig. 2 An example of measured velocity distribution about single drop.

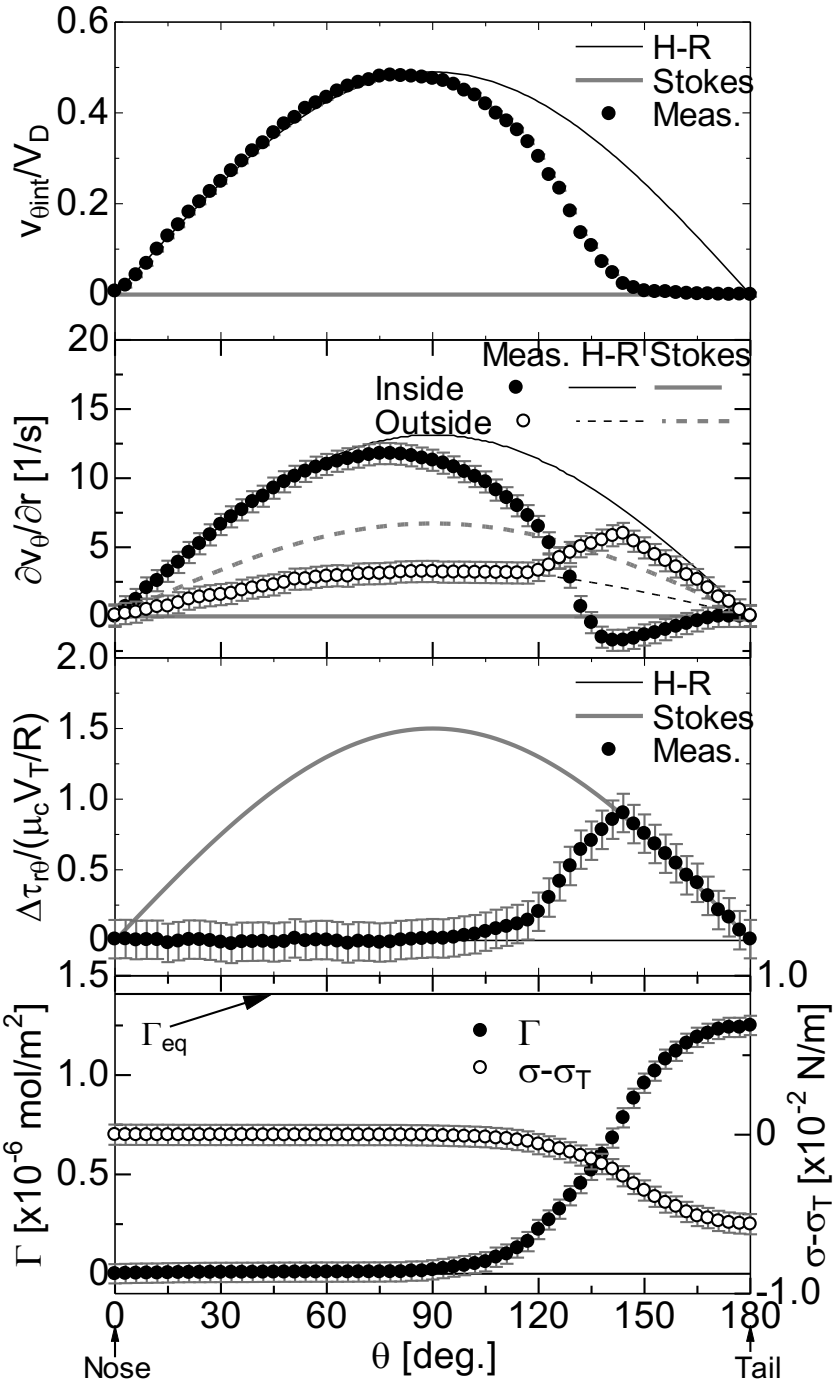

Fig. 3 Evaluation process of surfactant concentration.

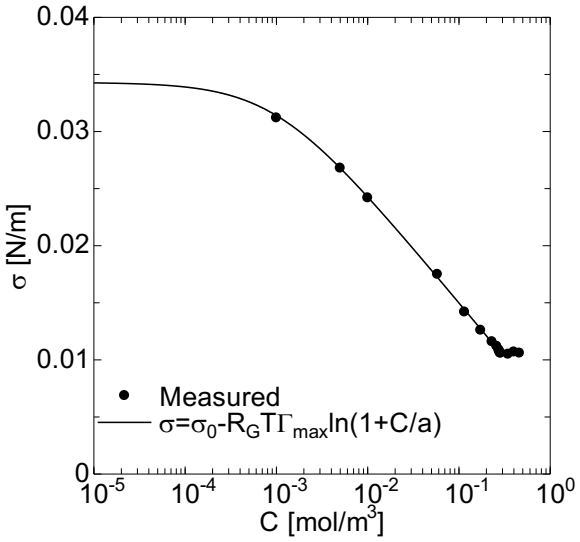

Fig. 4 Effect of *C* on σ.

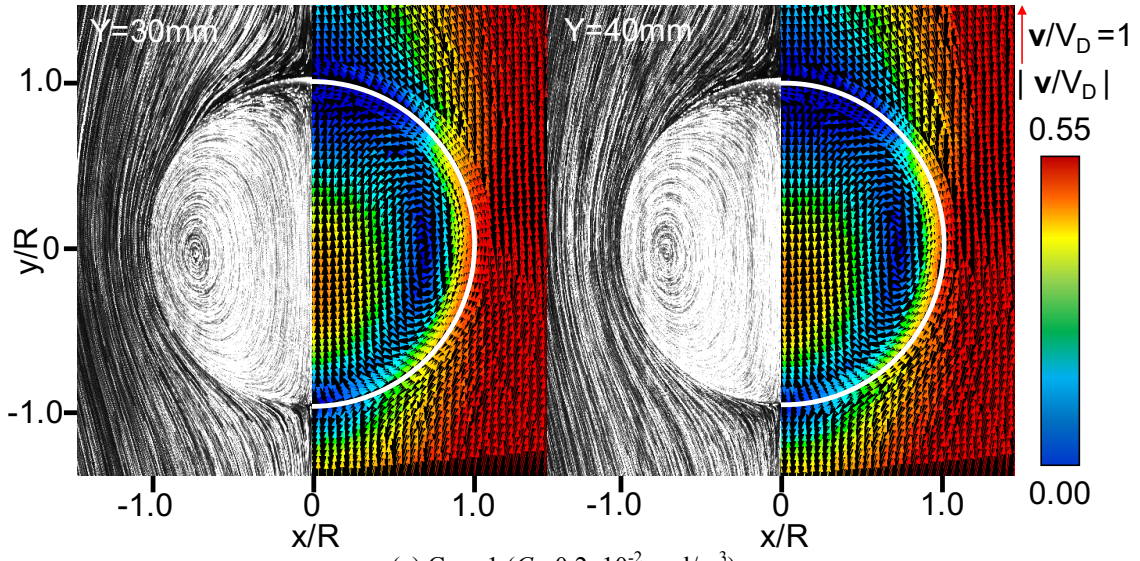

(a) Case 1 (C= 0.2x10^{-2} mol/m^3)

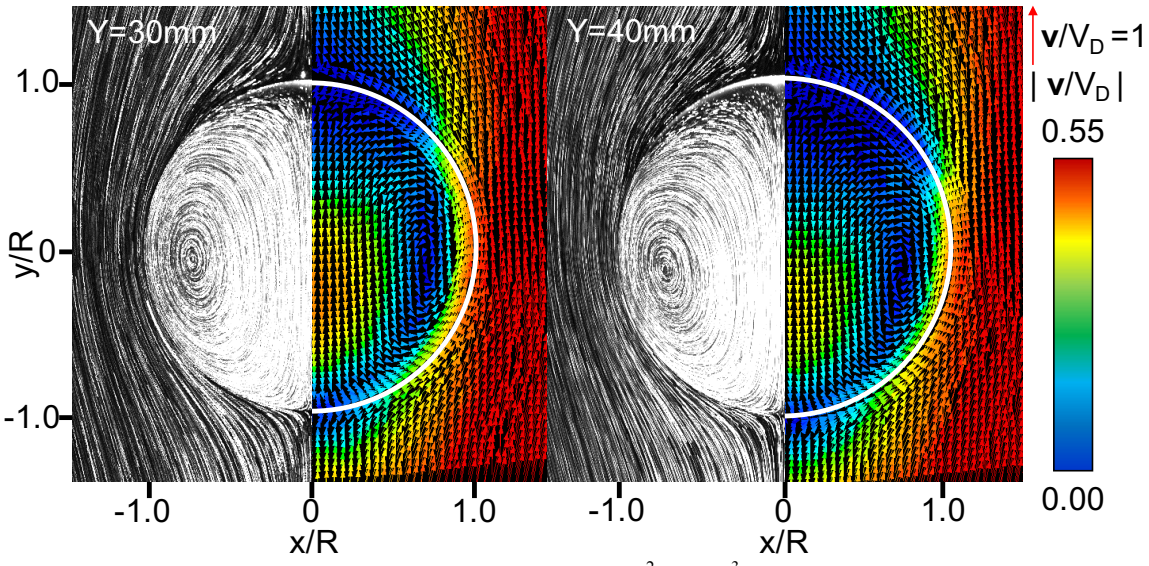

(b) Case 2 (C= 0.5x10^{-2} mol/m^3)

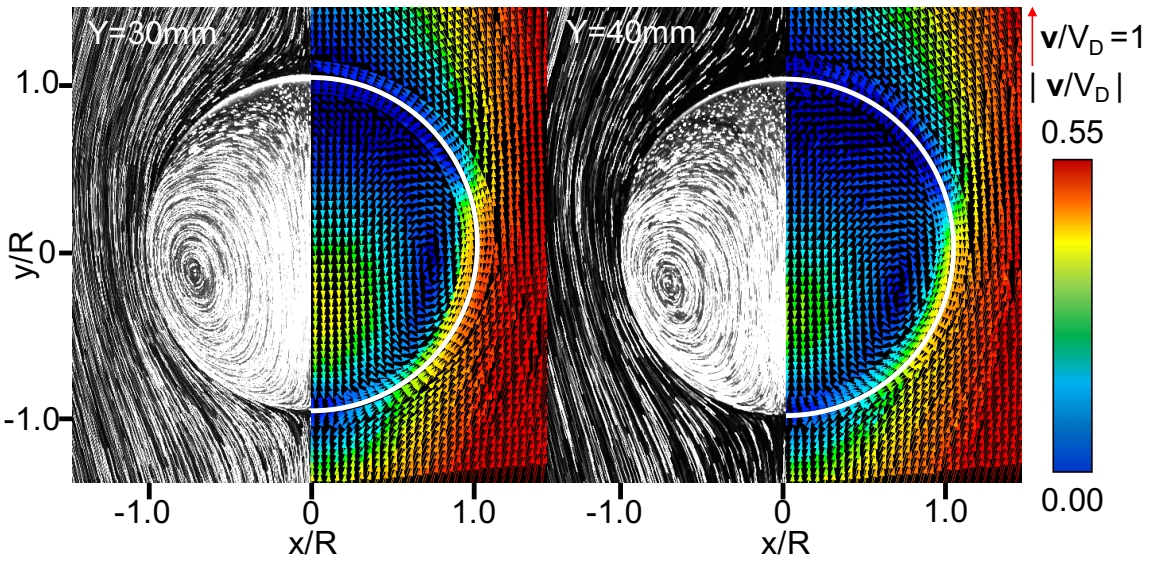

(c) Case 3 (C= 1.0x10^{-2} mol/m^3)

Fig. 5 Measured velocity distribution about a drop (left half: pathline, right half: velocity vector).

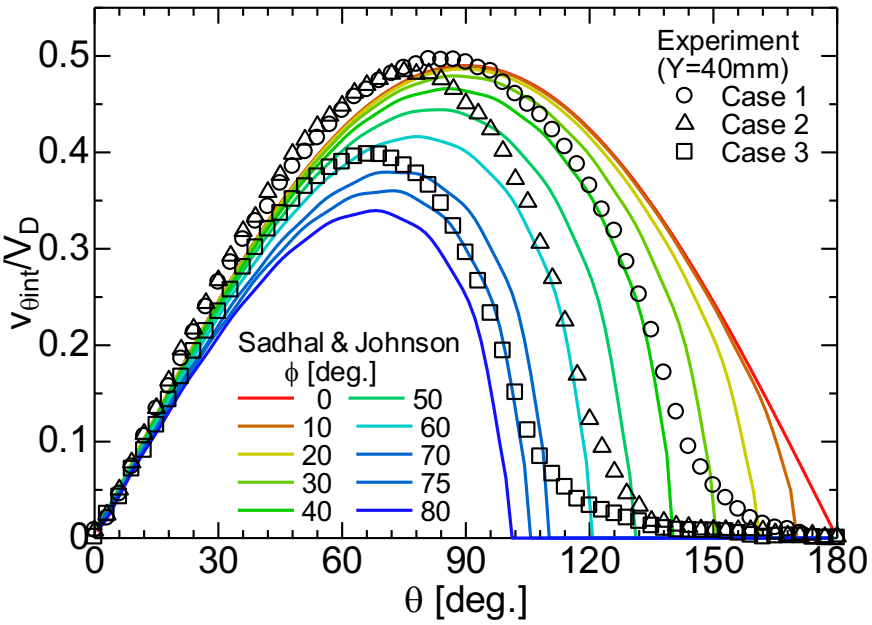

Fig. 6 Measured and theoretical interfacial velocities.

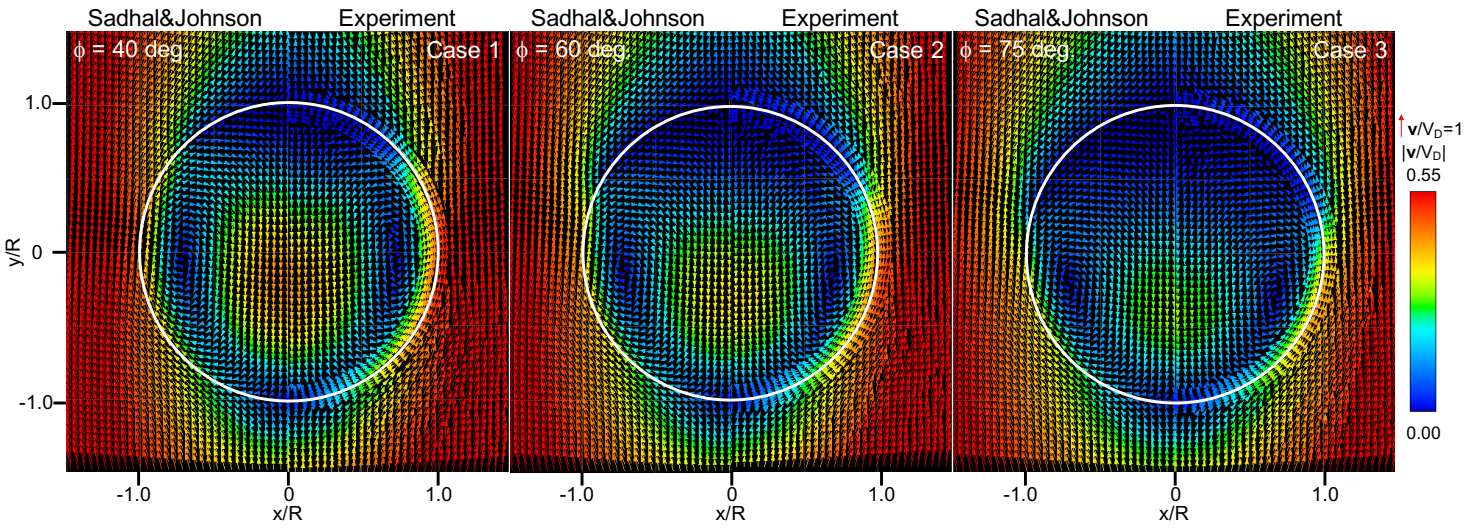

Fig. 7 Measured and theoretical velocity distributions about a drop.

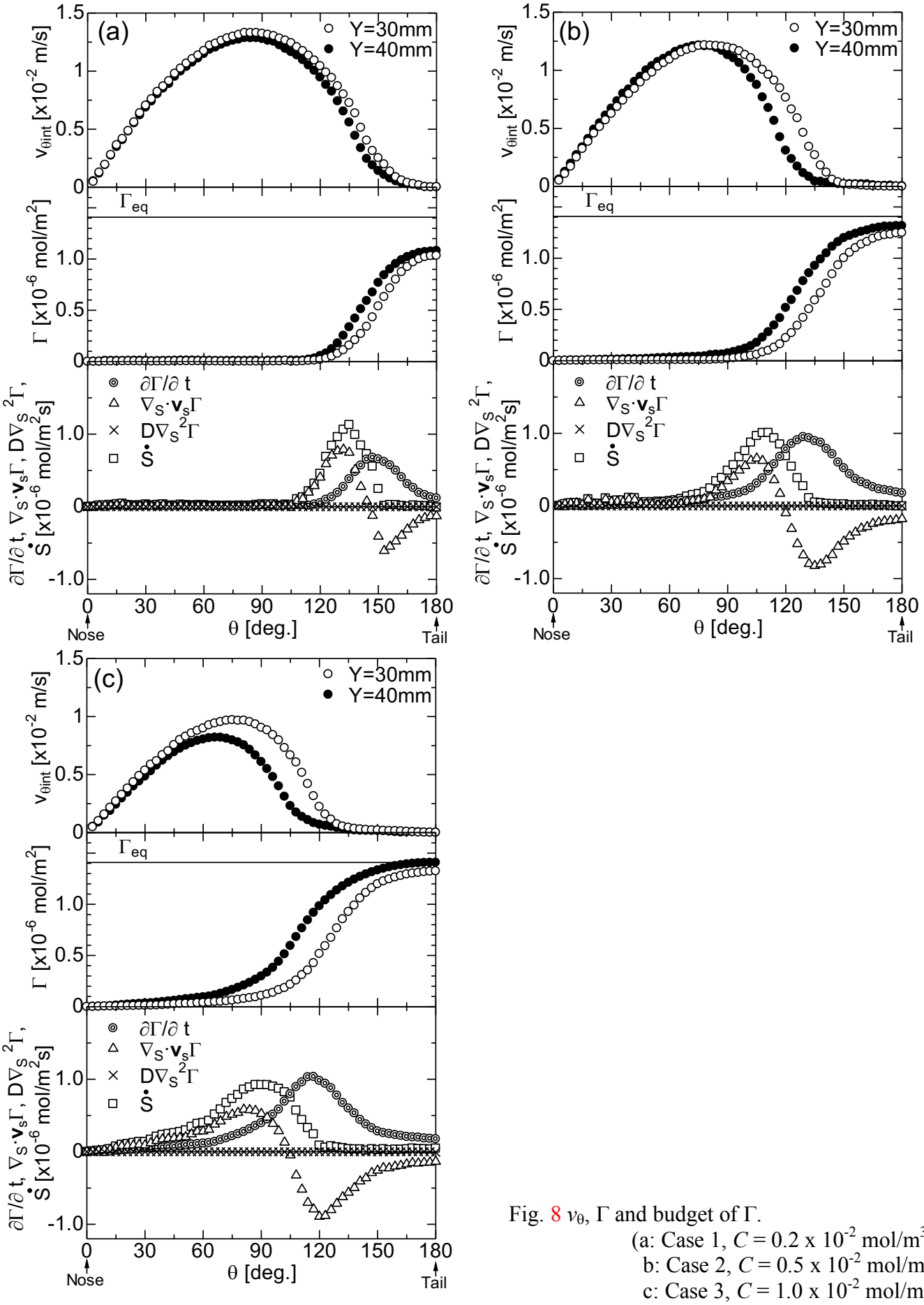

Fig. 8 v_θ, Γ and budget of Γ.
(a: Case 1, C = 0.2 x 10^{-2} mol/m^3,
b: Case 2, C = 0.5 x 10^{-2} mol/m^3,
c: Case 3, C = 1.0 x 10^{-2} mol/m^3)

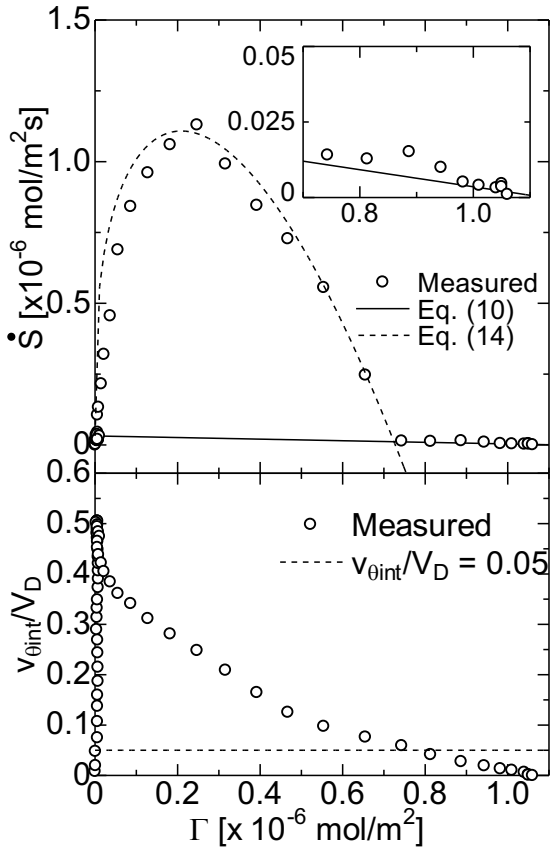

(a) Case 1 (C =0.2x10^{-2} mol/m^3)

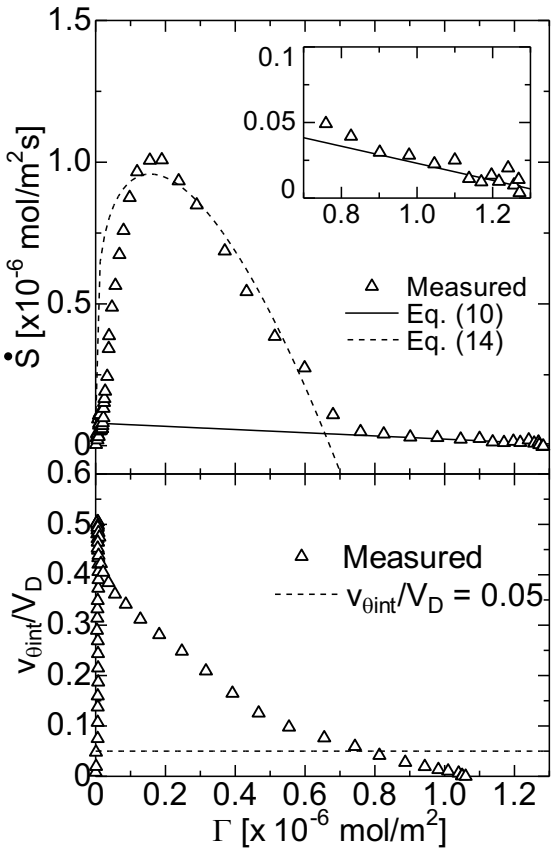

(b) Case 2 (C =0.5x10^{-2} mol/m^3)

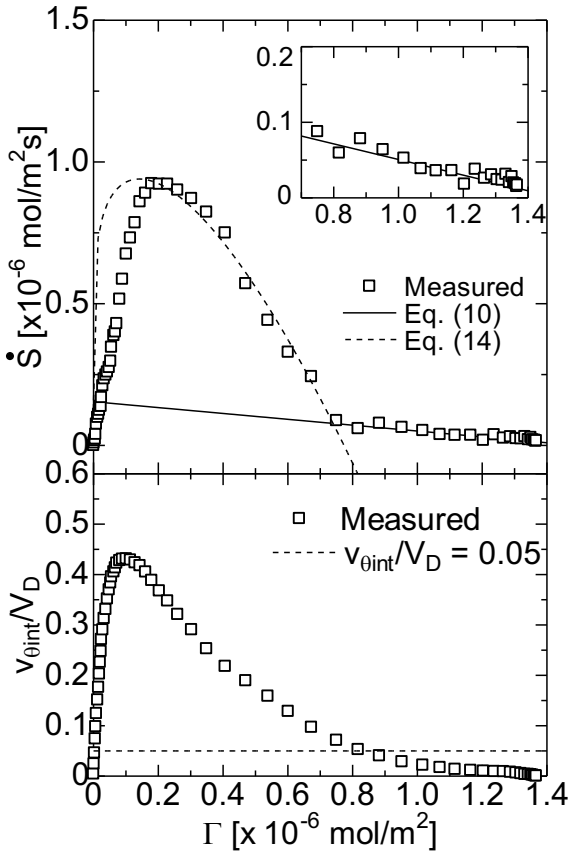

(c) Case 3 (C =1.0x10^{-2} mol/m^3)

Fig. 9 Relationship between Γ and $\dot{S}$.

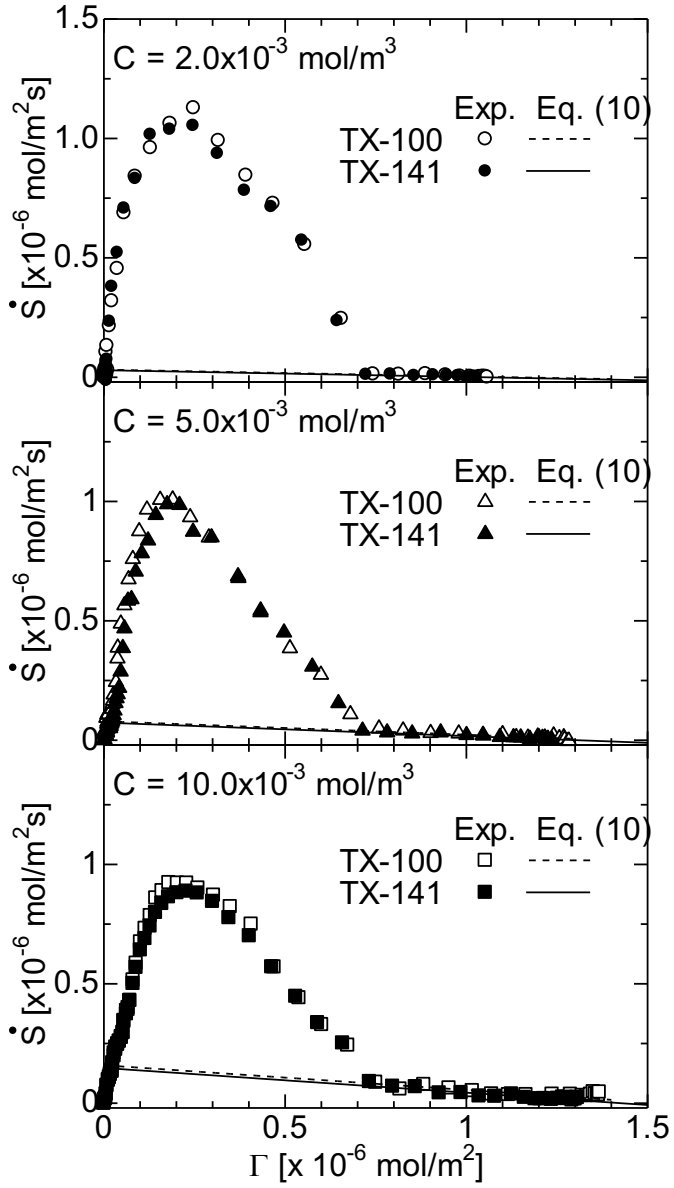

Fig. 10 Comparison of $\dot{S}$ between Triton X-100 and X-141.

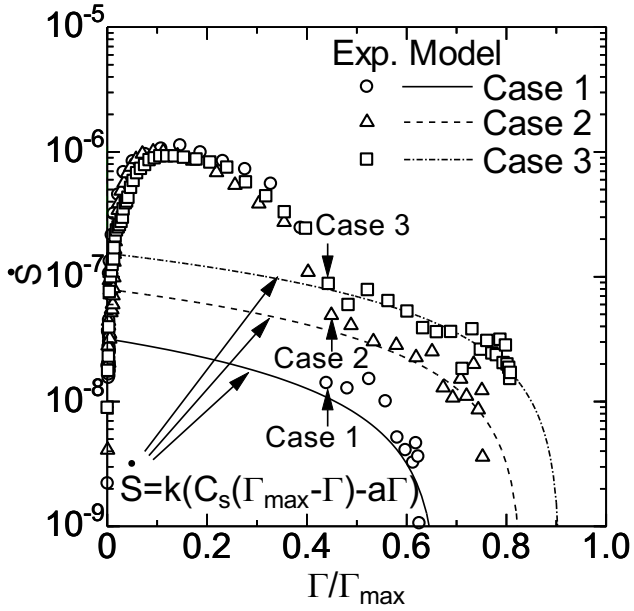

(a) Comparison among cases 1, 2 and 3

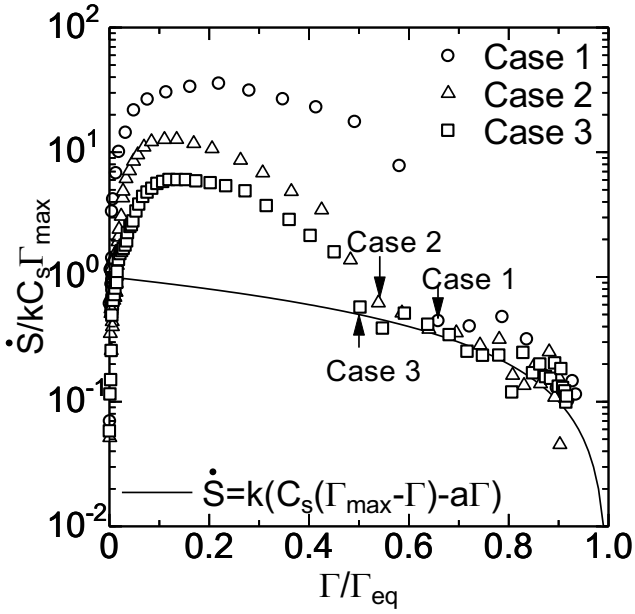

(b) Normalized $\dot{S}$ and Γ based on the Frumkin - Levich model

Fig. 11 Molar flux of surfactant due to adsorption and desorption

Table 1 Experimental conditions

	Case 1		Case 2		Case 3	
y [mm]	30	40	30	40	30	40
C [mol/m^3]	2.0×10^{-3}		5.0×10^{-3}		1.0×10^{-2}	
D [mm]	8.3		8.3		8.3	
V_D [m/s]	0.0273	0.0266	0.0232	0.0229	0.0207	0.0205
Re ($=\rho_C V_D D/\mu_C$)	0.73	0.71	0.62	0.61	0.56	0.55

Table 2 Physical properties of surfactants

	Triton X-100	Triton X-141
M [g/mol]	647	537
Γ_{max} [mol/m^2]	1.69×10^{-6}	1.57×10^{-6}
k [m^3/mol/s]	9.4	9.3
a [mol/m^3]	1.0×10^{-3}	9.4×10^{-4}